materials

MDPI

Communication

Enhancement of Catalytic Activity and Stability of $La_{0.6}Ca_{0.4}Fe_{0.7}Ni_{0.3}O_{2.9}$ Perovskite with ppm Concentration of Fe in the Electrolyte for the Oxygen Evolution Reaction

Sergei V. Porokhin *, Victoria A. Nikitina and Artem M. Abakumov *

Center for Energy Science and Technology, Skolkovo Institute of Science and Technology, Nobel Street 3, 143026 Moscow, Russia; V.Nikitina@skoltech.ru

* Correspondence: sergei.porokhin@skoltech.ru (S.V.P.); a.abakumov@skoltech.ru (A.M.A.)

Abstract: The catalytic activity and stability of an iron-nickel based oxygen-deficient perovskite for the oxygen evolution reaction (OER) are drastically improved with the ppm additive of Fe ions to the alkaline electrolyte. The enhancement is attributed to a 1–2 nm restructured $Ni_{0.5}Fe_{0.5}O_x(OH)_{2-x}$ (oxy)hydroxide layer, as demonstrated with scanning transmission electron microscopy. $La_{0.6}Ca_{0.4}Fe_{0.7}Ni_{0.3}O_{2.9}$ shows almost a four-fold increase in OER activity after Fe addition relative to the as-prepared pristine electrolyte, which demonstrates the low Tafel slope of 44 ± 2.4 mV dec^{-1} and the superior intrinsic activity of 706 ± 71 A $g^{-1}{}_{oxide}$ at 1.61 V vs. RHE.

Keywords: oxygen evolution reaction; water splitting; perovskite; lattice oxygen mechanism

Citation: Porokhin, S.V.; Nikitina, V.A.; Abakumov, A.M. Enhancement of Catalytic Activity and Stability of $La_{0.6}Ca_{0.4}Fe_{0.7}Ni_{0.3}O_{2.9}$ Perovskite with ppm Concentration of Fe in the Electrolyte for the Oxygen Evolution Reaction. *Materials* **2021**, *14*, 6403. https://doi.org/10.3390/ma14216403

Academic Editor: Alberto Vertova

Received: 29 September 2021
Accepted: 22 October 2021
Published: 26 October 2021

Efficient water electrolysis is highly desirable for economic branches where pure hydrogen and/or oxygen are used, for instance, in the transport sector with fuel cell electric vehicles, metallurgy (metal processing), and medicine. In the near future, stable constant growth in the consumption of pure hydrogen and oxygen as environmentally friendly sustainable resources is expected [1,2]. To meet the demand for economically viable clean production with renewable energy sources, it is necessary to increase the energy efficiency of water electrolysis by reducing the anodic overvoltage of the oxygen evolution reaction (OER), which is the rate-determining reaction in electrochemical water splitting.

Layered double hydroxide and perovskite materials have long been regarded as efficient OER electrocatalysts under alkaline conditions [3–8]. In particular, Ni-Fe-based oxide catalysts are well-studied and recognized materials for water electrolysis in alkaline media (for OER), which at certain conditions even outperform the electrocatalysts based on noble Ir, Ru elements [9,10]. The mechanism beneath high catalytic performance is related to lattice oxygen evolution reaction (LOER), which is characteristic of complex metal oxides (including perovskites). In light of recent studies [11,12], LOER is now seen as a fundamental process resulting in surface reconstruction towards highly active transition metal (oxy)hydroxides due to shallow perovskite A-site dissolution and B-site cation dissolution/re-deposition [13–16].

The fact that a small amount of Fe adsorbed from the electrolyte strongly affects OER activity and the stability of catalysts has already been reported for (Ni,Fe,Co)O_xH_y materials [17,18]. Rationalizing this observation is of extreme importance for the further design of efficient OER catalysts, as commercial electrolytes used for alkaline water electrolysis always contain Fe traces (typically around 1 ppm) [19,20], with the Fe content in most cases being poorly controlled under conventional experimental conditions. Recently, it has been shown that the surface of perovskite-type oxides can be deliberately modified with active (oxy)hydroxide layers by the addition of a small amount of Fe^{3+} ions to the electrolyte solution. When (oxy)hydroxide layers are deposited on the surface of oxides such as $Ba_{0.5}Sr_{0.5}Co_{0.8}Fe_{0.2}O_{3-\delta}$, $SrTi_{0.1}Fe_{0.85}Ni_{0.05}O_{3-\delta}$ [16,21,22], and $LaNiO_3$ [9,23], OER activity and stability demonstrates synergistic enhancement. This indicates that for perovskite

catalysts capable of undergoing LOER-induced surface reconstruction, the Fe species in the electrolyte are an essential component, as these species ensure the dynamically stable active sites in the surface (oxy)hydroxide layers [11,12]. Currently, further studies with the controlled addition of Fe species are needed for correct interpretation of electrochemical behavior of perovskite-based material in terms of activity–stability relationships.

In this work, we report on the enhanced OER catalytic activity of Ca-doped Ni/Fe-mixed perovskite with the additional presence of Fe ions in the electrolyte. This material has been demonstrated to possess promising OER activity due to the beneficial effect of Ca doping, which decreases the formation energy of the oxygen vacancies [24]. In this work, we search for strategies to further increase the activity and long-term stability of this material under the OER conditions. The $La_{0.6}Ca_{0.4}Fe_{0.7}Ni_{0.3}O_{2.9}$ (LCFN43) perovskite was prepared with a modified spray pyrolysis approach, as reported previously by our group [24]. Powder X-ray diffraction demonstrates a well-crystallized material with the perovskite-like *R*-3*c* structure with the unit cell parameters a = 5.4797(9) Å, c = 13.338(4) Å, V = 346.8(1) $Å^3$ (See Supplementary Figure S1).

Morphologically, the sample consists of porous hollow spherical particles with diameters ranging between 200 and 1200 (Figure 1) and with a BET specific surface area of 15 m^2g^{-1}. The spheres demonstrate mostly homogeneous cation distribution (Figure 1). The cation atomic ratio measured with energy-dispersive X-ray (EDX) analysis amounts to La:Ca:Fe:Ni = 0.58(1):0.41(1):0.70(1):0.31(1), which is in good agreement with the nominal composition. The oxygen content was determined using iodometric titration. Small particles with apparent Ca excess were also observed with EDX compositional mapping and attributed to the CaO impurity phase. This impurity, however, is washed out when soaking the sample in alkaline electrolyte [24], which allowed us to conduct the electrochemical measurements solely on the perovskite phase.

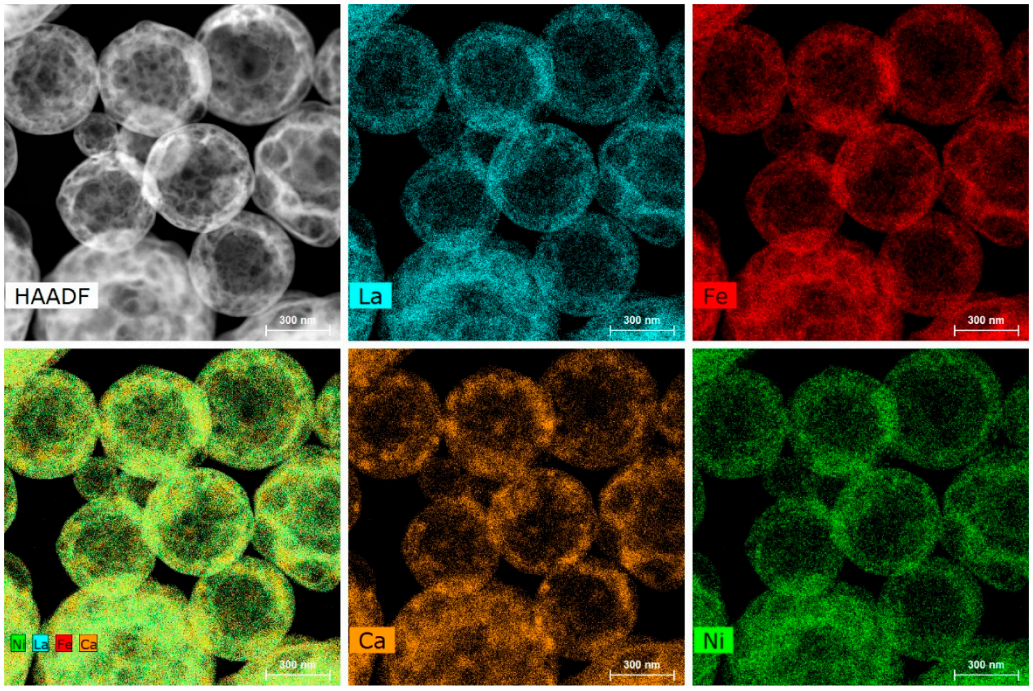

Figure 1. HAADF-STEM image of spherical hollow particles in the LCFN43 sample along with the La, Ca, Fe, Ni STEM-EDX maps and a mixed color-coded compositional map.

The OER activity of LCFN43 was evaluated in Ar-saturated 1M NaOH solution. Cyclic voltammograms (CVs) were registered within the potential limits of 0.93–1.66 V vs. RHE. The IR-corrected CVs in Figure 2a,b compare the current densities normalized to the geometric surface area of the rotating disk electrode (RDE). A much higher current density (12.9 mA cm^{-2} at 1.61 V RHE) was observed by adding Fe ions to the electrolyte in

1 ppm concentration, compared to the as-prepared pristine electrolyte (3.0 mA cm^{-2} at 1.61 V RHE). The Tafel slope in the Fe-modified electrolyte is significantly lower (44.0 ± 2.4 mV dec^{-1}), indicating faster reaction kinetics compared to 52.0 ± 2.6 mV dec^{-1} in the pristine electrolyte (Figure 2c).

The LCFN43 perovskite demonstrates a superior OER catalytic activity of 706 ± 71 A g^{-1}_{oxide} at 1.61 V vs. RHE, which is comparable to that (assuming 10% uncertainty) for $LaNiO_3$ covered with amorphous Ni-Fe (oxy)hydroxide, occurred after post-treatment by $FeCl_3$ (755 ± 76 A g^{-1}_{oxide}) [9] and pristine (Ni-Fe) hydroxides (600 ± 60 A g^{-1}_{oxide}) [25], and it outperforms other top perovskite catalysts, such as $Pr_{0.5}Ba_{0.3}Ca_{0.2}CoO_{3-\delta}$ (85 ± 9 A g^{-1}_{oxide}) [26] and $La_{0.4}Sr_{0.6}Ni_{0.5}Fe_{0.5}O_{3-\delta}$ (375 ± 38 A g^{-1}_{oxide}) [27] (Figure 2d).

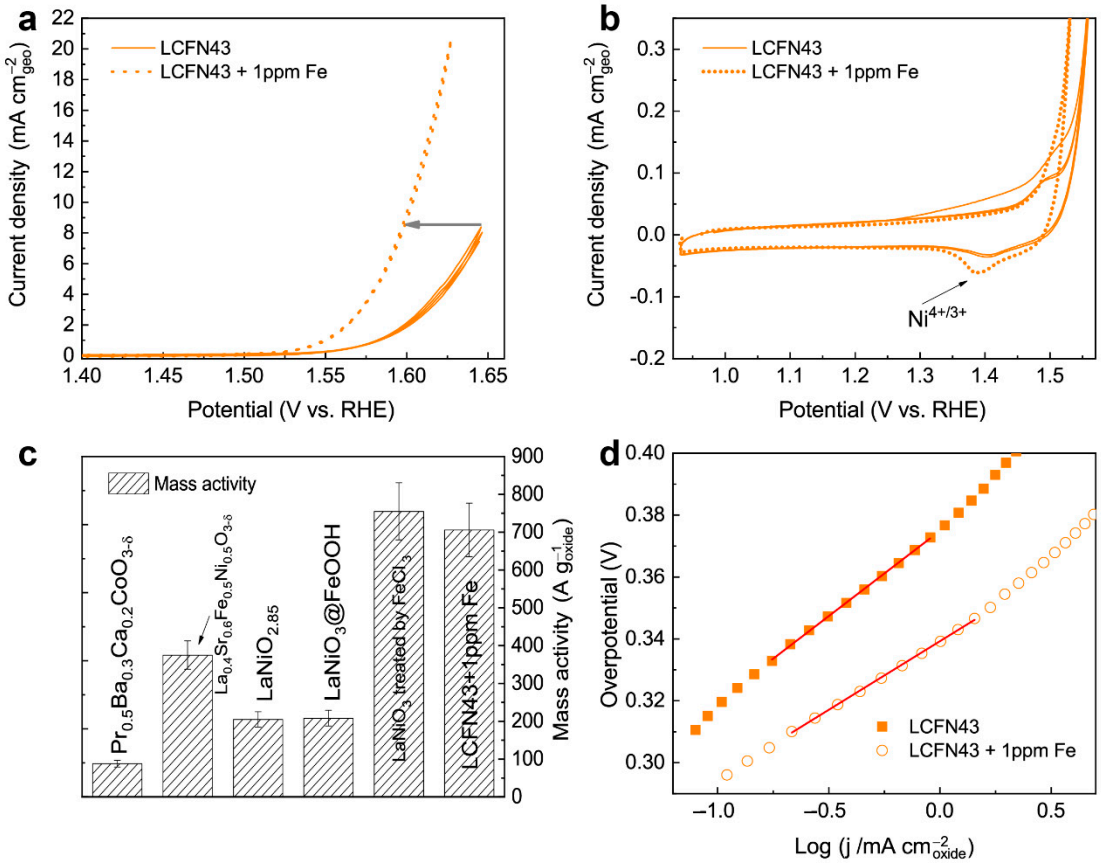

Figure 2. (**a**) CVs of the LCFN43 perovskite in the as-prepared pristine electrolyte and with the addition of 1 ppm Fe_{aq}, normalized to the geometric area of the electrode. (**b**) Enlarged regions of the CVs. (**c**) Mass activities at 1.61 V vs. RHE of LCFN43 + Fe_{aq} and comparison with other OER catalysts [9,23,26–28]. (**d**) Tafel plots for LCFN43 in the as-prepared pristine electrolyte and with the addition of 1 ppm Fe_{aq}. Measurement conditions: Ar-saturated 1M NaOH solution at 10 mV s^{-1} and 1600 rpm, total mass loading, 35.7 μg cm^{-2}, 50 wt.% Vulcan carbon XC72R.

We also measured the initial amount of Fe ions in aqueous 50 wt.% solution of NaOH (Sigma-Aldrich, Saint-Louis, MO, USA) by ICP-AES and observed 1200 μg L^{-1} concentration that corresponds to 63.4 μg L^{-1} (~0.063 ppm) in the as-prepared pristine 1M NaOH electrolyte. Therefore, 1 ppm of Fe is a significant addition that substantially improves the OER activity. Moreover, the potentials of the $Ni^{4+/3+}$ redox peaks were slightly shifted after immersion in 1 ppm Fe_{aq} electrolyte (Figure 2b) [18,29,30], evidencing that Fe incorporates/adsorbs on the surface, increasing the capacity of the cathodic peak, which is related to the formation of a thicker or more redox active Ni-Fe (oxy)hydroxide layer [8,30]. The LCFN43 sample demonstrates an activity improvement factor (ratio of current values in the 1 ppm Fe_{aq} electrolyte and in the pristine electrolyte) equal to 3.9. Such improvement, however, was not achieved immediately, but after 20 h of soaking the LCFN43 electrode in the

pristine electrolyte. If the measurements were performed without preliminary soaking or additional cycling, the improvement factor was 2.5 for the very first CV cycles, suggesting that the enhancement depends on pretreatment history, which in turn affects the surface composition [8,25]. For instance, improvement of OER activity in the $La_{1-x}Sr_xCoO_3$ (x = 0, 0.3) system steadily rises with cycling in KOH-based electrolyte deliberately containing 0.1 ppm of Fe_{aq} compared to the Fe-free solution, reaching after 1000 cycles the improvement factor of ~4 [12], similar to 3.9 in our case. Additionally, the NiO catalyst has also been tested in similar conditions with added $Fe(NO_3)_3$, demonstrating a 2.3-fold increase in OER activity [31].

To test the effect of Fe addition on the long-term stability of LCFN43 performance, the electrode consisting of perovskite catalyst mixed with 50 wt.% Vulcan carbon XC72R (VC) was polarized galvanostatically in a stepwise mode with the 32.6, 56, 78, 56, and 32.6 A g^{-1}_{oxide} current densities for at least 14 h (Figure 3a,b). The lower mass loading compared to the CV tests was used to maximize the homogeneity of catalyst coating, i.e., particle wetting and connectivity in the working environment. The relatively low current densities for the stability test were chosen to avoid high overvoltages, causing VC corrosion and oxygen bubble formation during OER.

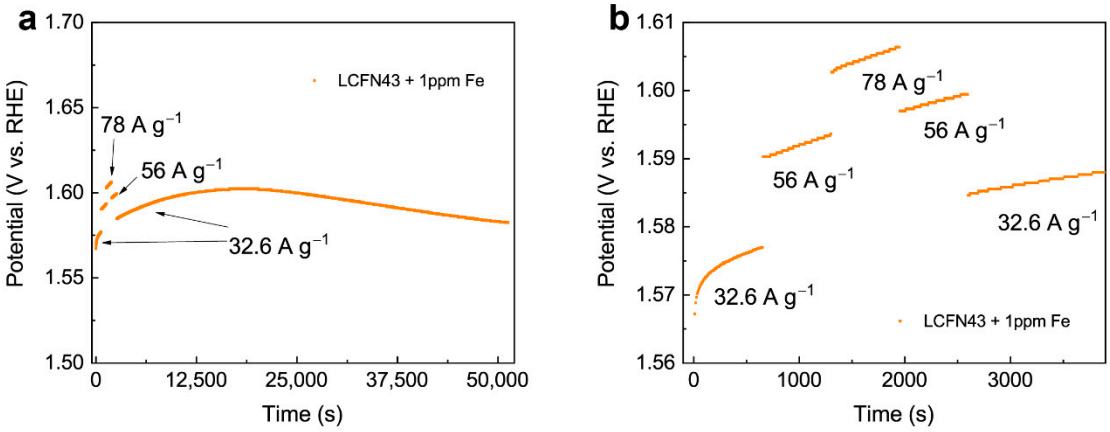

Figure 3. (**a**) Constant current test on LCFN43 in 1 ppm Fe_{aq} electrolyte at stepwise changes of the current density from 32.6 to 56, 78, and back to 56 and 32.6 A g^{-1}_{oxide}. (**b**) Enlarged regions of the first 3900 s of the test. Measurement conditions: Ar-saturated 1M NaOH solution, 1600 rpm, mass loading 18 μg cm^{-2}, 50 wt.% VC.

The potential slope slightly increases during the constant current test in a stepwise mode at short experimental times (up to 3900 s, Figure 3b). Further, the slope continues increasing and finally stabilizes at ~15,500 s, which suggests the shallow A-cation leaching and restructuring of the surface at the initial stage [24] and then the formation of dynamic equilibrium between Fe dissolution from perovskite during OER and redeposition promoted by Fe_{aq} in the electrolyte. This dynamic stability of active sites (Fe exchange) prevents deep structural changes of the perovskite particles [11,12]. After 21,000 s, the overpotential starts decreasing continuously, and this suggests an increase in the number of active surface centers that enhance the OER activity. A completely different behavior with a sharp increase in overpotential during galvanostatic polarization was observed for LCFN43 without the addition of Fe to the electrolyte (Figure S2).

In order to obtain deeper insight into the changes of the perovskite surface, the LCFN43 sample was collected directly from the electrode after the constant current test. The electrode was rinsed with deionized water, then with isopropanol, and then the thin catalyst film was scraped off with a micropipette and further transferred onto the TEM grid.

On the very surface of the perovskite particles after the constant current test, a thin restructured layer is observed (Figure 4a). The layer is 1–2 nm thick; it is not entirely amorphous and contains ordered nanoparticles. One of the nanoparticles (outlined in Figure 4a and enlarged in Figure 4b) demonstrates a hexagonal arrangement of cationic columns

with variable intercolumn distance with an average value of 2.9(3) Å. This corresponds well to the 001 projection of the *P*-3*m*1 crystal structure of $Ni(OH)_2$ layered hydroxide [32]. In fact, the measured projected distance between the cationic columns is in between those in $Ni(OH)_2$ (3.13 Å) and in NiOOH (2.81 Å), which reflects that the actual structure is in between of hydroxide and oxyhydroxide. EDX-STEM compositional maps and intensity profiles demonstrate that the surface layer contains both Ni and Fe (Figure 4c,d) with the Ni:Fe ratio of 54(3):46(3). Thus, the restructured surface layer can be classified as a mixed $Ni_{0.5}Fe_{0.5}O_x(OH)_{2-x}$ (oxy)hydroxide with variable O/OH ratio.

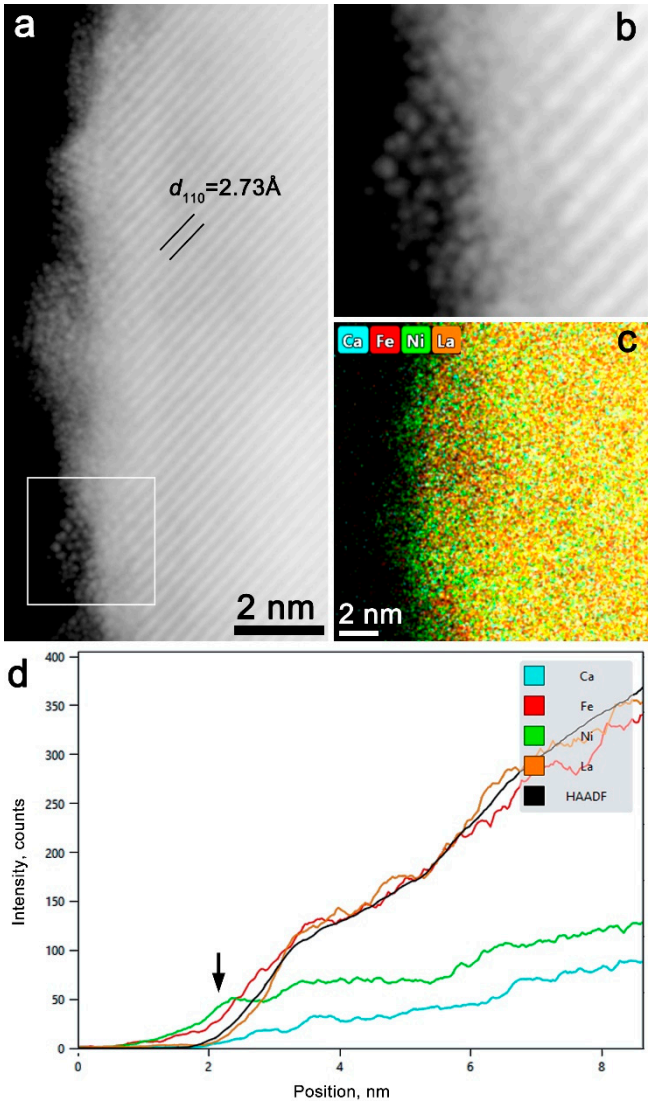

Figure 4. (**a**) HAADF-STEM image of the near-surface area in the LCFN43 sample after 14 h constant current test. The LCFN43 particle is visible by traces of the {110} crystal planes of the perovskite sub-cell with d ≈ 2.73 Å. A restructured surface layer with a thickness of 1–2 nm is visible. (**b**) Enlargement of the 001-oriented (Ni,Fe) (oxy)hydroxide nanoparticle in the restructured layer. (**c**,**d**) EDX-STEM compositional map and intensity profiles demonstrate that the surface layer (marked with the arrow) is Ni, Fe—enriched and La, Ca—depleted.

The CV and galvanostatic tests, along with the TEM data, allow us to conclude that the (oxy)hydroxide layer formed on the host (perovskite) surface under the OER conditions is responsible for the enhanced OER activity. The presence of Fe in the electrolyte stabilizes the dynamic active OER sites and prevents deep structural changes of the perovskite particles. In summary, the addition of 1 ppm of Fe into alkaline electrolyte creates a stable

dynamic (oxy)hydroxide interface with the host perovskite catalyst, thus increasing both the catalytic activity and the stability of the catalyst in oxygen evolution reaction.

Supplementary Materials: The following are available online at https://www.mdpi.com/article/10.3390/ma14216403/s1, Figure S1. PXRD profiles after Rietveld refinement of the pristine $La_{0.6}Ca_{0.4}Fe_{0.7}Ni_{0.3}O_{2.9}$ perovskite. The ticks indicate the Bragg reflection positions for the main perovskite phase (bottom row) and the CaO admixture (4.4(5) wt.%, top row). Figure S2. Constant current tests on LCFN43 in the electrolyte containing ppm amounts of Fe_{aq} (dark line) and in the as-prepared electrolyte (bright line). Experimental conditions: Ar-saturated 1M NaOH solution, 1600 rpm, mass loading 35.7 μg cm^{-2}, 50 wt.% VC. Materials and method: Synthesis, Powder X-ray diffraction, Transmission electron microscopy, Surface area analysis, Electrochemical measurements, Inductively coupled plasma atomic emission spectroscopy.

Author Contributions: Conceptualization, S.V.P., V.A.N. and A.M.A.; investigation, S.V.P. and A.M.A.; writing—original draft preparation; S.V.P. and A.M.A.; writing—review and editing, S.V.P., V.A.N. and A.M.A.; supervision, V.A.N. and A.M.A. All authors have read and agreed to the published version of the manuscript.

Funding: This research received no external funding.

Institutional Review Board Statement: Not applicable.

Informed Consent Statement: Not applicable.

Data Availability Statement: Data available on request.

Acknowledgments: The authors thank Ivan Mikheev for the ICP-AES analysis of electrolyte. S.V.P. acknowledges the support from Skolkovo Institute of Science and Technology. Access to the TEM facilities has been granted by AICF of Skoltech.

Conflicts of Interest: The authors declare no conflict of interest.

References

1. David, M.; Ocampo-Martínez, C.; Sánchez-Peña, R. Advances in alkaline water electrolyzers: A review. *J. Energy Storage* **2019**, *23*, 392–403. [CrossRef]
2. Staffell, I.; Scamman, D.; Velazquez Abad, A.; Balcombe, P.; Dodds, P.E.; Ekins, P.; Shah, N.; Ward, K.R. The role of hydrogen and fuel cells in the global energy system. *Energy Environ. Sci.* **2019**, *12*, 463–491. [CrossRef]
3. Coletta, V.C.; Gonçalves, R.V.; Bernardi, M.I.B.; Hanaor, D.A.H.; Assadi, M.H.N.; Marcos, F.C.F.; Nogueira, F.G.E.; Assaf, E.M.; Mastelaro, V.R. Cu-Modified SrTiO 3 Perovskites Toward Enhanced Water–Gas Shift Catalysis: A Combined Experimental and Computational Study. *ACS Appl. Energy Mater.* **2021**, *4*, 452–461. [CrossRef]
4. Matsumoto, Y.; Sato, E. Electrocatalytic properties of transition metal oxides for oxygen evolution reaction. *Mater. Chem. Phys.* **1986**, *14*, 397–426. [CrossRef]
5. Singh, R.N.; Jain, A.N.; Tiwari, S.K.; Poillerat, G.; Chartier, P. Physicochemical and electrocatalytic properties of $LaNiO_3$ prepared by a low-temperature route for anode application in alkaline water electrolysis. *J. Appl. Electrochem.* **1995**, *25*, 1133–1138. [CrossRef]
6. McCrory, C.C.L.; Jung, S.; Ferrer, I.M.; Chatman, S.M.; Peters, J.C.; Jaramillo, T.F. Benchmarking Hydrogen Evolving Reaction and Oxygen Evolving Reaction Electrocatalysts for Solar Water Splitting Devices. *J. Am. Chem. Soc.* **2015**, *137*, 4347–4357. [CrossRef] [PubMed]
7. Friebel, D.; Louie, M.W.; Bajdich, M.; Sanwald, K.E.; Cai, Y.; Wise, A.M.; Cheng, M.-J.; Sokaras, D.; Weng, T.-C.; Alonso-Mori, R.; et al. Identification of Highly Active Fe Sites in (Ni,Fe)OOH for Electrocatalytic Water Splitting. *J. Am. Chem. Soc.* **2015**, *137*, 1305–1313. [CrossRef] [PubMed]
8. Baeumer, C.; Li, J.; Lu, Q.; Liang, A.Y.L.; Jin, L.; Martins, H.P.; Duchoň, T.; Glöß, M.; Gericke, S.M.; Wohlgemuth, M.A.; et al. Tuning electrochemically driven surface transformation in atomically flat $LaNiO_3$ thin films for enhanced water electrolysis. *Nat. Mater.* **2021**, *20*, 674–682. [CrossRef] [PubMed]
9. Chen, G.; Zhu, Y.; Chen, H.M.; Hu, Z.; Hung, S.; Ma, N.; Dai, J.; Lin, H.; Chen, C.; Zhou, W.; et al. An Amorphous Nickel–Iron-Based Electrocatalyst with Unusual Local Structures for Ultrafast Oxygen Evolution Reaction. *Adv. Mater.* **2019**, *31*, 1900883. [CrossRef] [PubMed]
10. Zhu, Y.-X.; Jiang, M.-Y.; Liu, M.; Wu, L.-K.; Hou, G.-Y.; Tang, Y.-P. An Fe–V@NiO heterostructure electrocatalyst towards the oxygen evolution reaction. *Nanoscale* **2020**, *12*, 3803–3811. [CrossRef] [PubMed]
11. Chung, D.Y.; Lopes, P.P.; Farinazzo Bergamo Dias Martins, P.; He, H.; Kawaguchi, T.; Zapol, P.; You, H.; Tripkovic, D.; Strmcnik, D.; Zhu, Y.; et al. Dynamic stability of active sites in hydr(oxy)oxides for the oxygen evolution reaction. *Nat. Energy* **2020**, *5*, 222–230. [CrossRef]

12. Lopes, P.P.; Chung, D.Y.; Rui, X.; Zheng, H.; He, H.; Martins, P.F.B.D.; Strmcnik, D.; Stamenkovic, V.R.; Zapol, P.; Mitchell, J.F.; et al. Dynamically stable active sites from surface evolution of perovskite materials during the oxygen evolution reaction. *J. Am. Chem. Soc.* **2021**, *143*, 2741–2750. [CrossRef] [PubMed]
13. Zhao, J.W.; Shi, Z.X.; Li, C.F.; Ren, Q.; Li, G.R. Regulation of Perovskite Surface Stability on the Electrocatalysis of Oxygen Evolution Reaction. *ACS Mater. Lett.* **2021**, *3*, 721–737. [CrossRef]
14. Wu, T.; Sun, S.; Song, J.; Xi, S.; Du, Y.; Chen, B.; Sasangka, W.A.; Liao, H.; Gan, C.L.; Scherer, G.G.; et al. Iron-facilitated dynamic active-site generation on spinel $CoAl_2O_4$ with self-termination of surface reconstruction for water oxidation. *Nat. Catal.* **2019**, *2*, 763–772. [CrossRef]
15. Fabbri, E.; Nachtegaal, M.; Binninger, T.; Cheng, X.; Kim, B.-J.; Durst, J.; Bozza, F.; Graule, T.; Schäublin, R.; Wiles, L.; et al. Dynamic surface self-reconstruction is the key of highly active perovskite nano-electrocatalysts for water splitting. *Nat. Mater.* **2017**, *16*, 925–931. [CrossRef] [PubMed]
16. Kim, B.J.; Cheng, X.; Abbott, D.F.; Fabbri, E.; Bozza, F.; Graule, T.; Castelli, I.E.; Wiles, L.; Danilovic, N.; Ayers, K.E.; et al. Highly Active Nanoperovskite Catalysts for Oxygen Evolution Reaction: Insights into Activity and Stability of $Ba_{0.5}Sr_{0.5}Co_{0.8}Fe_{0.2}O_{2+\delta}$ and $PrBaCo_2O_{5+\delta}$. *Adv. Funct. Mater.* **2018**. [CrossRef]
17. Enman, L.J.; Stevens, M.B.; Dahan, M.H.; Nellist, M.R.; Toroker, M.C.; Boettcher, S.W. Operando X-Ray Absorption Spectroscopy Shows Iron Oxidation Is Concurrent with Oxygen Evolution in Cobalt–Iron (Oxy)hydroxide Electrocatalysts. *Angew. Chem. Int. Ed.* **2018**, *57*, 12840–12844. [CrossRef] [PubMed]
18. Trotochaud, L.; Young, S.L.; Ranney, J.K.; Boettcher, S.W. Nickel–Iron Oxyhydroxide Oxygen-Evolution Electrocatalysts: The Role of Intentional and Incidental Iron Incorporation. *J. Am. Chem. Soc.* **2014**, *136*, 6744–6753. [CrossRef] [PubMed]
19. Klaus, S.; Cai, Y.; Louie, M.W.; Trotochaud, L.; Bell, A.T. Effects of Fe Electrolyte Impurities on $Ni(OH)_2/NiOOH$ Structure and Oxygen Evolution Activity. *J. Phys. Chem. C* **2015**, *119*, 7243–7254. [CrossRef]
20. Corrigan, D.A. The Catalysis of the Oxygen Evolution Reaction by Iron Impurities in Thin Film Nickel Oxide Electrodes. *J. Electrochem. Soc.* **1987**, *134*, 337–384. [CrossRef]
21. Zhu, Y.; Chen, G.; Zhong, Y.; Chen, Y.; Ma, N.; Zhou, W.; Shao, Z. A surface-modified antiperovskite as an electrocatalyst for water oxidation. *Nat. Commun.* **2018**, *9*. [CrossRef] [PubMed]
22. Cheng, X.; Kim, B.-J.; Fabbri, E.; Schmidt, T.J. Co/Fe Oxyhydroxides Supported on Perovskite Oxides as Oxygen Evolution Reaction Catalyst Systems. *ACS Appl. Mater. Interfaces* **2019**, *11*, 34787–34795. [CrossRef] [PubMed]
23. Li, Z.; Lv, L.; Ao, X.; Li, J.G.; Sun, H.; An, P.; Xue, X.; Li, Y.; Liu, M.; Wang, C.; et al. An effective method for enhancing oxygen evolution kinetics of $LaMO_3$ (M = Ni, Co, Mn) perovskite catalysts and its application to a rechargeable zinc–air battery. *Appl. Catal. B Environ.* **2020**, *262*. [CrossRef]
24. Porokhin, S.V.; Nikitina, V.A.; Aksyonov, D.A.; Filimonov, D.S.; Pazhetnov, E.M.; Mikheev, I.V.; Abakumov, A.M. Mixed-cation perovskite $La_{0.6}Ca_{0.4}Fe_{0.7}Ni_{0.3}O_{2.9}$ as a stable and efficient catalyst for the oxygen evolution reaction. *ACS Catal.* **2021**, *11*, 8338–8348. [CrossRef]
25. Louie, M.W.; Bell, A.T. An investigation of thin-film Ni-Fe oxide catalysts for the electrochemical evolution of oxygen. *J. Am. Chem. Soc.* **2013**, *135*, 12329–12337. [CrossRef] [PubMed]
26. He, D.; He, G.; Jiang, H.; Chen, Z.; Huang, M. Enhanced durability and activity of the perovskite electrocatalyst $Pr_{0.5}Ba_{0.5}CoO_{3-\delta}$ by Ca doping for the oxygen evolution reaction at room temperature. *Chem. Commun.* **2017**, *53*, 5132–5135. [CrossRef] [PubMed]
27. Guo, Q.; Li, X.; Wei, H.; Liu, Y.; Li, L.; Yang, X.; Zhang, X.; Liu, H.; Lu, Z. Sr, Fe co-doped perovskite oxides with high performance for oxygen evolution reaction. *Front. Chem.* **2019**, *7*, 224. [CrossRef] [PubMed]
28. Jin, Y.; Huo, W.; Zhang, L.; Li, Y.; Chen, Q.; Zhang, X.; Yang, S.; Nie, H.; Zhou, X.; Yang, Z. $NaBH_4$-reduction induced tunable oxygen vacancies in $LaNiO_{2.7}$ to enhance the oxygen evolution reaction. *Chem. Commun.* **2021**, *57*, 7168–7171. [CrossRef]
29. Kawashima, K.; Márquez-Montes, R.A.; Li, H.; Shin, K.; Cao, C.L.; Vo, K.M.; Son, Y.J.; Wygant, B.R.; Chunangad, A.; Youn, D.H.; et al. Electrochemical behavior of a Ni_3N OER precatalyst in Fe-purified alkaline media: The impact of self-oxidation and Fe incorporation. *Mater. Adv.* **2021**, *2*, 2299–2309. [CrossRef]
30. Krivina, R.A.; Ou, Y.; Xu, Q.; Twight, L.P.; Stovall, T.N.; Boettcher, S.W. Oxygen Electrocatalysis on Mixed-Metal Oxides/Oxyhydroxides: From Fundamentals to Membrane Electrolyzer Technology. *Acc. Mater. Res.* **2021**, *2*, 548–558. [CrossRef]
31. Nardi, K.L.; Yang, N.; Dickens, C.F.; Strickler, A.L.; Bent, S.F. Creating Highly Active Atomic Layer Deposited NiO Electrocatalysts for the Oxygen Evolution Reaction. *Adv. Energy Mater.* **2015**, *5*, 1500412. [CrossRef]
32. Kazimirov, V.Y.; Smirnov, M.B.; Bourgeois, L.; Guerlou-Demourgues, L.; Servant, L.; Balagurov, A.M.; Natkaniec, I.; Khasanova, N.R.; Antipov, E.V. Atomic structure and lattice dynamics of Ni and Mg hydroxides. *Solid State Ion.* **2010**, *181*, 1764–1770. [CrossRef]